Temperature-resonant cyclotron spectra in confined geometries

A. Pototsky,[1] P. Hänggi,[2] F. Marchesoni,[3] and S. Savel'ev[4]
[1]*Department of Mathematics, University of Cape Town, Rondebosch 7701, South Africa*
[2]*Institut für Physik, Universität Augsburg, D-86135 Augsburg, Germany*
[3]*Dipartimento di Fisica, Università di Camerino, I-62032 Camerino, Italy*
[4]*Department of Physics, Loughborough University, Loughborough LE11 3TU, United Kingdom*
(Received 15 February 2011; published 11 July 2011)

We consider a two-dimensional gas of colliding charged particles confined to finite size containers of various geometries and subjected to a uniform orthogonal magnetic field. The gas spectral densities are characterized by a broad peak at the cyclotron frequency. Unlike for infinitely extended gases, where the amplitude of the cyclotron peak grows linearly with temperature, here confinement causes such a peak to go through a maximum for an optimal temperature. In view of the fluctuation-dissipation theorem, the reported resonance effect has a direct counterpart in the electric susceptibility of the confined magnetized gas.

DOI: 10.1103/PhysRevE.84.011107 PACS number(s): 05.40.−a, 52.20.−j, 76.20.+q

I. INTRODUCTION

Electronic fluctuations are of great importance in plasma physics due to their relevance in charge and energy transport [1] and to the well-established connection between fluctuation spectra and electronic susceptibility [2]. As the temperature of the system is increased, the power of thermal fluctuations contained in any narrow frequency interval is also expected to increase. However, such a straightforward temperature dependence has been observed in systems where the electron dynamics is incoherent as a result of the electron interactions with other electrons, positively charged ions, and impurities. If, however, the electron dynamics also contains a coherent component such as rotation with cyclotron frequency in the presence of a magnetic field, then the temperature dependence of the fluctuation power spectra may develop nontrivial resonant behaviors. For instance, it has been demonstrated [3] that a magnetized plasma operated at the limit-cycle fixed-point bifurcation point and driven by a tunable external white noise undergoes stochastic resonance [4]. In contrast, the observation that in constrained geometries the matching of thermal scales and characteristic system length can produce detectable resonant effects has been previously reported [5,6].

In this paper we show that a simpler instance of temperature controlled resonance can naturally occur in a confined magnetized electron gas due to the matching of two lengths: the electron intrinsic thermal length, or gyroradius, and the finite system size. The effect investigated here should not be mistaken for a manifestation of the well known electron cyclotron resonance, which results instead from the matching of two frequencies: the cyclotron frequency of an electron moving in a uniform magnetic field and the pump frequency of a perpendicular ac electric field [7]. The dynamics of a magnetoplasma electron can be reduced to the two-dimensional (2D) Brownian motion of a charged particle subjected to a uniform magnetic field. In Sec. II we analyze the power spectral density (PSD) of a magnetized Brownian particle moving in an unconstrained planar geometry. We notice in particular that the amplitude of the cyclotron peak grows linearly with temperature. At variance with this remark, in Sec. III our numerical simulations show that in constrained geometries the cyclotron peak goes through a maximum for an optimal temperature (Sec. III A), which in turn is determined by the matching of system size and (temperature-dependent) average cyclotron radius (Sec. III B). In Sec. IV we also show that the observed resonant temperature dependence of the cyclotron peak is robust with respect to variations of the boundary conditions and the geometry of the system. Finally, in Sec. V we discuss possible applications of this effect to confined systems of magnetocharges in biological and artificial structures.

II. UNBOUNDED ELECTRON GAS

In an equilibrium neutral plasma electrons of charge q and mass m oscillate with characteristic angular frequency [8] $\omega_p = (n_0 q^2/m\varepsilon_0)^{1/2}$ (in SI notation), where n_0 is the average electron density and ϵ_0 is the vacuum permittivity. In the following we restrict ourselves to weakly magnetized plasmas to ensure that the cyclotron frequency associated with B_0, ω_c, is much smaller than ω_p, i.e., $\omega_c = qB_0/m \ll \omega_p$. This allows us to reduce the dynamics of a magnetoplasma electron to the 2D Brownian motion of a charged particle subjected to a uniform magnetic field. This is a long-standing problem in plasma and astroparticle physics [9–11]. Here we limit ourselves to introducing the results relevant to the discussion of our simulation data. The corresponding Langevin equation reads

$$\begin{aligned} \mathbf{v} &= \dot{\mathbf{r}}, \\ \dot{\mathbf{v}} &= \frac{q}{m}(\mathbf{v}\times\mathbf{B}_0) - \gamma\mathbf{v} + \sqrt{2\gamma\frac{kT}{m}}\boldsymbol{\xi}(t), \end{aligned} \tag{1}$$

where the vector $\boldsymbol{\xi}(t) = (\xi_x(t),\xi_y(t))$ represents two independent Gaussian white noises with $\langle\xi_i(t)\rangle = 0$ and $\langle\xi_i(t)\xi_i(0)\rangle = \delta(t)$ for $i = x,y$.

For numerical purposes, it is convenient to rescale both time, $t \to \omega_c t$, and space, $r \to r/\lambda$. We recall that ω_c is the B_0-dependent cyclotron angular frequency and λ is the T-dependent electron gyroradius $\lambda = \sqrt{kT/m\omega_c^2}$ [8]. In dimensionless units Eq. (1) reads

$$\begin{aligned} \dot{\mathbf{r}} &= \mathbf{v}, \\ \dot{\mathbf{v}} &= \mathbf{v}\times\mathbf{b}_0 - g\mathbf{v} + \sqrt{2g}\boldsymbol{\xi}(t), \end{aligned} \tag{2}$$

where $\mathbf{b}_0$ is a unit vector parallel to $\mathbf{B}_0$. Note that, in the absence of boundaries, the only free parameter in the dimensionless Langevin equation [Eq. (2)] is the scaled damping constant $g = \gamma/\omega_c$. In the following all results will be given in dimensional units for the readers' convenience.

For the linear and unconstrained dynamics of Eq. (2) the PSD $S(\omega) = \langle|\hat{\mathbf{r}}(\omega)|^2\rangle$, with $\hat{\mathbf{r}}(\omega)$ representing the Fourier transform of $\mathbf{r}(t)$, can be computed analytically by means of standard harmonic analysis [12,13]. Taking advantage of the fact that $\xi_x(t)$ and $\xi_y(t)$ are uncorrelated white Gaussian noises, we obtain

$$S_x(\omega) = S_y(\omega) = \frac{S_{v_x}}{\omega^2},$$
$$S_{v_x}(\omega) = \frac{2kT}{m}\frac{\gamma(\omega^2+\gamma^2)(\omega^2+\gamma^2+\omega_c^2)}{\gamma^2\left(\omega^2+\gamma^2+\omega_c^2\right)^2+\omega^2\left(\omega^2+\gamma^2-\omega_c^2\right)^2}, \tag{3}$$

where S_i and S_{v_i} denote the PSD of the $i = x,y$ components of the 2D vectors $\mathbf{r}$ and $\mathbf{v}$, respectively. Note that at resonance $\omega = \omega_c$, the peak of the transverse velocity is $S_{v_x}(\omega_c) = v_{\rm th}^2/2\gamma$, with $v_{\rm th}^2 = \langle\mathbf{v}^2\rangle = 2kT/m$. In view of the discussion below, we note here that the stationary autocorrelation function of the velocity, $G(t-t') = \langle v_x(t)v_x(t')\rangle = \langle v_y(t)v_y(t')\rangle$, solely depends on the difference $t-t'$ and is related to the inverse Fourier transform of the PSD $S_{v_x}(\omega)$ through the Wiener-Khinchin theorem [10–13],

$$G(t-t') = \langle v_x(t)v_x(t')\rangle = \frac{1}{2\pi}\int_{-\infty}^{\infty} S_{v_x}(\omega)e^{i\omega(t-t')}d\omega$$
$$= \frac{kT}{m}e^{-\gamma|t-t'|}\cos\left[\omega_c(t-t')\right]. \tag{4}$$

For an unbounded planar electron gas, the stationary distribution density of the velocity is Maxwellian [9–11] and does not depend on either the damping constant γ or the magnetic field B_0,

$$f(\mathbf{v}) = \frac{m}{2\pi kT}\exp\left(-\frac{m\mathbf{v}^2}{2kT}\right). \tag{5}$$

The autocorrelation function of the electron coordinates $\langle\mathbf{r}(t)\mathbf{r}(t')\rangle$ diverges as a function of t and t' because the free motion of electrons on the plane is unbounded.

In this regard it should be noted that the diffusion of a Brownian charge carrier on a plane perpendicular to a constant magnetic field is normal, that is, for asymptotically large t, $\langle\mathbf{r}^2\rangle = 4D_Bt$ with

$$D_B = \frac{kT}{m\gamma}\frac{\gamma^2}{\gamma^2+\omega_c^2}. \tag{6}$$

This means that for $B_0 > 0$ the particle diffusivity gets suppressed, as D_B is smaller than the free diffusion coefficient $D_0 = kT/m\gamma$.

The typical velocity PSD $S_{v_x}(\omega)$ and an example of a velocity autocorrelation function $G(t)$ are depicted in Fig. 1 for different values of the damping constant γ. The peak at the cyclotron frequency ω_c broadens as γ is increased. In the remaining sections of this paper we choose γ to be much smaller than ω_c, i.e., $\gamma \ll \omega_c$. This ensures that the cyclotron peak is well pronounced or, equivalently, that electrons with any given velocity v tend to perform many cyclotron orbits of radius $r_c = v/\omega_c$ before being perturbed by the combined action of noise and friction. Accordingly, in the underdamped limit the diffusion coefficient D_B tends to $kT\gamma/m\omega_c^2 = \lambda^2\gamma$.

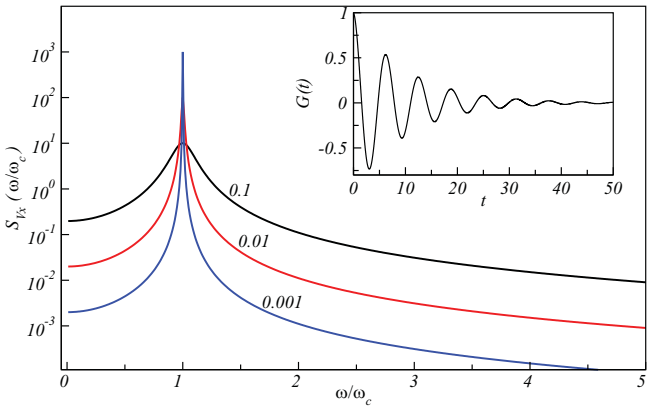

FIG. 1. (Color online) Power spectral density $S_{v_x}(\omega) = S_{v_y}(\omega)$ [Eq. (3)] for $kT/m = 1$, $\omega_c = 1$, and different γ (reported in the legend). The inset shows the velocity correlation function of Eq. (4), $G(t)$, for $\gamma = 0.1$.

III. FINITE SYSTEMS

Our goal now is to compute the PSD $S(\omega)$ of a confined 2D gas of electrons with finite temperature and for different geometries and boundary conditions. It should be noticed that $S(\omega)$ encodes important information about the electromagnetic transmission properties of the electron gas. In fact, $S(\omega)$ can be directly linked to the imaginary part of the gas electric susceptibility $\kappa(\omega)$ via the fluctuation-dissipation relation $S(\omega) \sim kT\,\mathrm{Im}[\kappa(\omega)]$ [2].

We start with the simplest case of an electron gas trapped in a strip delimited by two walls parallel to the y axis and a fixed distance d apart. Electrons are assumed to be reflected elastically by the strip boundaries, which leads to a zero net transverse flux in the x direction.

We numerically integrated the dimensionless Langevin equation [Eq. (2)] for g in the range 10^{-3}–10^{-2} and then restored dimensional units with $\omega_c = 1$ and fixed system size. With respect to the time unit, this corresponds to reporting ω in units of ω_c, with no severe restriction on the actual value of B_0, but for the condition that $\omega_c \ll \omega_p$ (see Secs. II and V for more details). With respect to the space units, setting the width of the strip to a given value d makes the electron PSDs depend explicitly on the temperature, which had been eliminated from Eq. (2) by expressing all lengths in units of λ. Note that in our plots $\omega_c = 1$, so that the scaled temperature kT/m boils down to the square of the gyroradius λ, introduced in Sec. II.

A. Resonant cyclotron peak

The typical PSDs of the transverse coordinate $S_x(\omega)$ are depicted in the main panel of Fig. 2. The finely dotted curves represent $S_x(\omega)$, as computed numerically through Eq. (2) with $\gamma = 0.005$ and ideal reflecting boundaries located at $x = \pm d/2$ with $d = 1$. The solid curves are the corresponding $S_x(\omega)$ for an unbounded planar electron gas, as predicted in

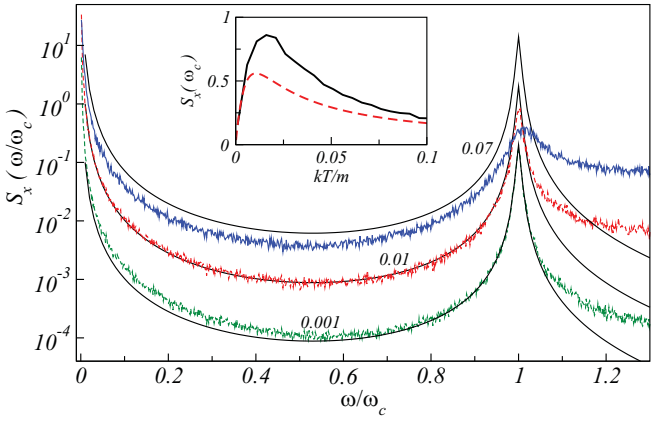

FIG. 2. (Color online) Transverse power spectral density $S_x(\omega)$ of an electron moving in a strip of width $d = 1$ (see sketch in Fig. 3), as computed from Eq. (2) for $\gamma = 0.005$, $\omega_c = 1$, and the scaled temperature kT/m reported in the legend. Solid curves represent the corresponding PSDs for an unbounded planar system. Inset: Amplitude of the cyclotron peak $S_x(\omega_c)$ as a function of kT/m (solid curve) and its analytical approximation [Eq. (8)] (dashed curve). Note that for $\omega_c = 1$ the scaled temperature kT/m coincides with λ^2.

Eq. (3). The height and the width of the cyclotron peak depend on the scaled temperature kT/m.

Unlike for the case of an infinite system, the amplitude of the cyclotron peak $S_x(\omega_c)$ for the confined electron gas depends resonantly on the temperature, as shown in the inset of Fig. 2: As T is gradually increased, $S_x(\omega_c)$ goes through a maximum for an optimal temperature T_c whose dependence on the confinement geometry is investigated in the following sections. This behavior may be reminiscent of stochastic resonance [4]. However, we anticipate that here the optimal temperature is defined by the matching of two length scales, rather than two time scales, as it is the case in ordinary stochastic resonance [4,14]. Finite volume effects have been reported in the early stochastic resonance literature [15], but in a totally different context.

B. Quantitative interpretation

The resonant temperature dependence of the cyclotron peak can be qualitatively explained as follows. First we recall that, in the underdamped regime, the diffusion time of a charged Brownian particle across a strip of width d is strongly suppressed by the presence of a magnetic field, especially for $\gamma t \ll 1$. From Eq. (43) of Ref. [10], $\langle \mathbf{r}^2 \rangle = \mathcal{O}(t^3)$; hence the transverse diffusion time in the strip can be safely assumed to be much shorter than the cyclotron period, as illustrated in Figs. 3(a) and 3(b). We notice that, as the interaction of the electrons with the walls is elastic, the equilibrium distribution of their velocity is not affected by the boundary geometry and is still given by the Maxwell distribution of Eq. (5).

Moreover, the cyclotron radius of an electron moving with instantaneous velocity v is $r_c = v/\omega_c$; in the regime of low damping $\gamma \ll \omega_c$, we can neglect the effects of friction on the electron orbits. This means that the contribution to S_x from a circular orbit of constant radius r_c is proportional to $r_c^2/2\gamma$ [see the discussion following Eq. (3)], that is, it increases quadratically with v. However, this conclusion applies only

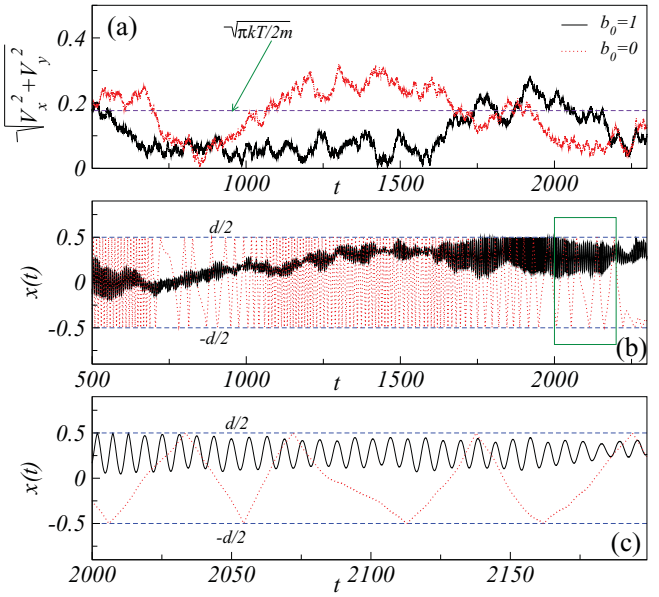

FIG. 3. (Color online) Trajectory samples of (a) $|\mathbf{v}|(t)$ and (b) and (c) $x(t)$ for $kT/m = 0.02$, $\gamma = 10^{-3}$, $d = 1$, and $\omega_c = 1$ (black curves) or $B_0 = 0$ [red (gray) curves]. Shown in (c) is a blowup of the trajectory portion marked by a rectangle in (b). The horizontal dashed line in (a) represents $\langle |\mathbf{v}| \rangle$ as computed from Eq. (7).

to electronic trajectories with centers located a distance not smaller than r_c away from the reflecting boundaries. Indeed, when the electrons come too close to the boundaries, they repeatedly bounce off the walls, so that their trajectories get distorted [see Fig. 3(c)]. For an equilibrium distribution of the electron velocities, this surely happens when their orbit diameter is larger than half the strip width, $2r_c > d/2$.

In view of the preceding arguments, we assume for simplicity that fast electrons with too large a cyclotron radius, say, $r_c > d/4$, do not contribute to the cyclotron peak, whereas only a fraction $1 - 4r_c/d$ of the slower electrons with $r_c < d/4$ do. On further noticing that from Eq. (5) the equilibrium distribution of v is

$$\rho(v) = \frac{mv}{kT} \exp\left(-\frac{mv^2}{2kT}\right), \tag{7}$$

we obtain the estimate for the amplitude of the cyclotron peak,

$$S_x(\omega_c) \simeq \frac{(\bar{T}d)^2}{32\gamma}\left[2 + e^{-(1/2\bar{T}^2)} - 3\sqrt{\frac{\pi}{2}}\,\bar{T}\,\mathrm{erf}\left(\frac{1}{\sqrt{2\bar{T}^2}}\right)\right], \tag{8}$$

where $\bar{T} = 4\sqrt{kT/m}/d\omega_c$ and $\mathrm{erf}(\cdots)$ denotes the standard error function. Note that this estimate for $S_x(\omega_c)$ systematically underestimates the corresponding simulation curve as we neglected the residual contribution from electronic orbits larger, but not much larger, than $d/4$. By numerically evaluating Eq. (8), one concludes that both the resonance value of the cyclotron peak $S_{\max}(\omega_c)$ and T_c grow quadratically with d, namely, $kT_c/m \simeq 0.01(\omega_c d)^2$ and $S_{\max}(\omega_c) \simeq 2.8 \times 10^{-3} d^2/\gamma$.

We also stress that the emergence of a resonant cyclotron peak is not conditioned by the elastic boundary assumption. Boundary randomness or fluctuations may indeed affect the

residual contribution from large electronic orbits with $r_c > d/4$, but not the bulk contribution estimated in Eq. (8).

IV. DEPENDENCE ON GEOMETRY AND BOUNDARY CONDITIONS

Next we numerically compute $S_x(\omega_c)$ as a function of the temperature for different geometries and boundary conditions in order to demonstrate the robustness of the temperature resonance of the cyclotron peak. We consider here five confining setups for the 2D electron gas.

(i) Box with an internal semitransparent wall. We consider a $d \times d$ square box, centered at the origin $x = y = 0$, and containing a semitransparent internal wall $x = h$ with $|h| < d/2$, parallel to the y axis. The internal wall acts like a porous filter letting charges pass through only if the x component of their velocity v_x is larger than a certain threshold velocity v_c, i.e., $v_x > v_c$. If $v_x \leqslant v_c$, the electrons are elastically reflected back into their half box. We fix $d = 12$ and $h = 0$ and plot in Fig. 4(a) the amplitude of the cyclotron peak as a function of the scaled temperature kT/m for different values of the threshold. For $v_c = 0$ the compartment wall is transparent, so that the effective width of the box is d, whereas for $v_c > 5$ the internal wall acts as an almost perfectly reflective boundary, thus dividing the square box in two rectangular compartments of width $d/2$. Despite the different geometries, confined cyclotron orbits are confirmed to generate a resonant temperature dependence of the electronic PSD, no matter what v_c is. Moreover, in agreement with our analytical discussion of the infinite strip from Sec. III B, the optimal temperature T_c, corresponding to the maxima of the plotted curves, diminishes

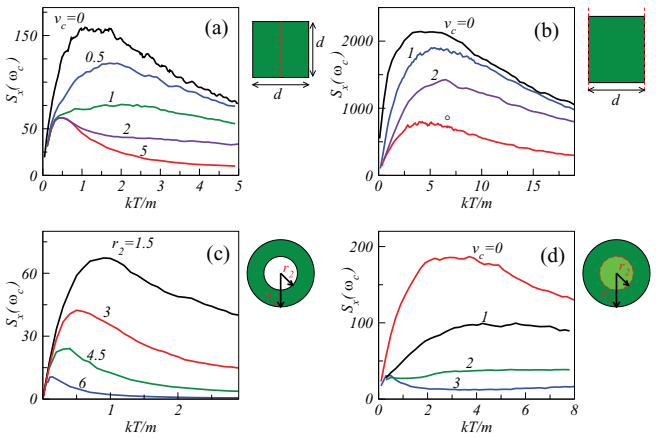

FIG. 4. (Color online) Amplitude of the cyclotron peak $S_x(\omega_c)$ as a function of the scaled temperature kT/m for the different geometries of Sec. IV as sketched. In all four panels $\omega_c = 1$ and $\gamma = 1.66 \times 10^{-3}$ [(a) and (b)] and 0.003 [(c) and (d)]. (a) Square box containing a semitransparent wall $x = h$ [case (i)]. The simulation parameters are $d = 12$, $h = 0$, and threshold velocity v_c as reported next to the relevant data sets. (b) Infinite strip with semitransparent walls [case (ii)]. The simulation parameters are $d = 18$ and v_c as reported next to the relevant data sets. (c) Annulus with reflective inner boundary [case (iii)] with $v_c = \infty$. The outer radius is kept constant, $r_1 = 9$, and the inner radius r_2 varied as in the legend. (d) Same geometry as in (c) but with constant inner radius $r_2 = 4.5$ and semitransparent inner wall with threshold velocity v_c in the legend [case (iv)].

with $d^2 \to d^2/4$ by a factor 4 on increasing v_c from 0 to ∞ and thus halving the container width.

(ii) Infinite strip with semitransparent walls. Let us consider the infinite strip of Sec. III A with the important difference that now its parallel walls are semitransparent, as described in (i). If $v_x \leqslant v_c$ the electrons are contained in the strip; if $v_x > v_c$ the electrons exit one wall and reenter through the other one with periodic boundary conditions. In Fig. 4(b) the peak amplitude $S(\omega_c)$ is plotted as a function of the temperature for different values of the threshold. Since the boundaries are periodic for $v_c = 0$ and reflective for $v_c = \infty$, here our approximate estimate for $S(\omega_c)$ from Sec. III B is expected to work well only as $v_c \to \infty$. In this limit, Eq. (8) reproduces fairly closely both T_c and $S_{\max}(\omega_c)$. In the opposite limit of purely periodic boundary conditions, the cyclotron peak at resonance $S_{\max}(\omega_c)$ gets enhanced, while T_c only weakly depends on v_c.

(iii) Annulus with a reflecting inner wall and (iv) with a semitransparent inner wall. Next we consider electrons trapped in a circle with radius r_1, which represents an ideal reflecting boundary. The inner space is divided by a second circle of radius r_2, with $r_2 < r_1$, into two compartments. The inner circle is concentric with the outer circle and its circumference works as a semitransparent wall [case (iv)] with threshold velocity v_c (applied to the radial component of $\mathbf{v}$). The case (iii) of an ideal reflecting inner circle corresponds to setting the threshold velocity $v_c = \infty$ [see Fig. 4(c)]; the gas is confined to an annulus. As one can anticipate from the discussion in Sec. III B, the maximum of the cyclotron peak $S_{\max}(\omega_c)$ decreases on increasing r_2 [see Fig. 4(c)]. Correspondingly, the optimal temperature T_c also decreases because the width of the annulus shrinks. The dependence of the resonant cyclotron effect on v_c is illustrated in Fig. 4(d). The effect is most pronounced in the case of a perfectly transparent inner circle $v_c = 0$. Indeed, lowering v_c enlarges the surface accessible to the cyclotron orbits of the confined electrons. As suggested by Eq. (8), T_c and the maximum of $S(\omega_c)$ grow quadratically with the effective transverse dimensions of the gas container; for the simulation parameters reported in Fig. 4(d), this corresponds to an increase of both quantities by a factor of about 4 as v_c increases from 0 to ∞.

(v) Infinite strip with an internal semitransparent wall. Finally, we show that by appropriately choosing the geometry of the system, the cyclotron peak can go through two maxima as a function of temperature. Such a double resonance was found by inserting an internal wall, $x = h$ with $|h| < d/2$, of tunable threshold v_c in the infinite strip of Sec. III A. Our simulation results for a symmetric geometry with $d = 12$, $h = 0$, and different v_c are displayed in Fig. 5(a). The limiting regimes $v_c = 0$ and $v_c \to \infty$ are reproduced well by our approximate formula in Eq. (8). In the intermediate regimes, say at $v_c = 2$, the $S(\omega_c)$ features two maxima. The low temperature maximum is centered around the optimal temperature $T_c^{(\infty)}$ corresponding to a partitioned strip $v_c = \infty$. Most remarkably, the optimal temperature of the second maximum on the right is systematically higher than the optimal temperature $T_c^{(0)}$ of the unpartitioned strip $v_c = 0$. Moreover, such a double resonance could only be found for certain combinations of v_c and h/d, as shown in Fig. 5(b).

The occurrence of a double resonance can be explained by noticing that for electrons with $v_x \leqslant v_c$ the wall acts as an

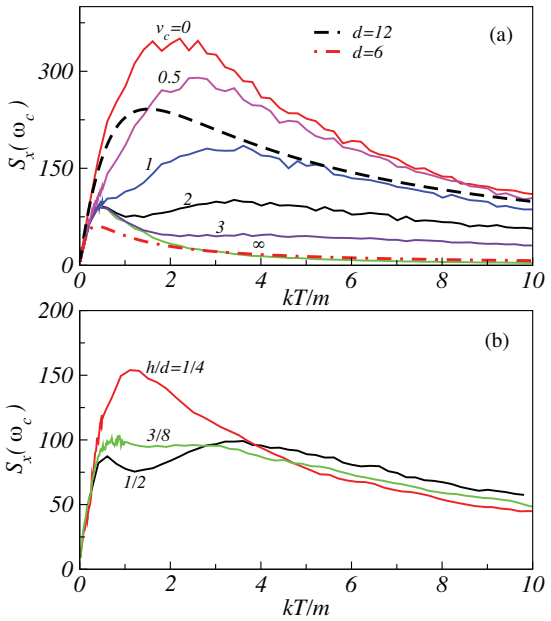

FIG. 5. (Color online) Amplitude of the cyclotron peak $S_x(\omega_c)$ as a function of the scaled temperature kT/m [case (v) of Sec. IV] for $\omega_c = 1$ and $\gamma = 1.66 \times 10^{-3}$. (a) Infinite strip of width $d = 12$ with a semitransparent filter located at $h = 0$ and different thresholds v_c (in the legend). The curves of Eq. (8) for $d = 12$ (dashed) and 6 (dash-dotted) are reported for a comparison. (b) Same geometry as in (a), but for $v_c = 2$ and different h (in the legend).

effective partition. In Fig. 5(a), where $h = 0$, this corresponds to splitting the strip into two equal strips of half width. Correspondingly, the slow electrons trapped in either half strip contribute a cyclotron peak that is the highest for $T \simeq T_c^{(\infty)}$. Fast electrons with $v_x > v_c$ are free to move across the full width of the strip so that the optimal temperature of their cyclotron orbits ought to approach $T_c^{(0)}$ with $T_c^{(0)} \simeq 4T_c^{(\infty)}$. However, by taking a closer look at our derivation of Eq. (8), it is apparent that in the case of fast electrons the lower limit of the integral must be modified to account for the condition $v_x > v_c$. As a consequence of the bell shaped profile of the Maxwell distribution, such a modification of the integration range moves the optimal value $\bar{T}_c$ to appreciably higher values, in agreement with Fig. 5.

V. CONCLUDING REMARKS

The temperature controlled resonance of the cyclotron spectra, emerging from a matching between the system size length d with the thermal electron gyroradius λ, becomes detectable for a confined magnetized gas of charged particles under two important conditions, summarized by the inequalities $\gamma \ll \omega_c \ll \omega_p$. The condition $\omega_c \ll \omega_p$, introduced in Sec. II, required applying magnetic fields of relatively low intensity. The underdamped regime $\gamma \ll \omega_c$ was assumed to enhance the cyclotron peak of the transverse PSD $S_x(\omega)$ over its background. Both conditions can be met in magnetoplasmas [1].

In normal metals the observation of the resonant cyclotron effects reported here might seem impossible. At room temperature typical values of the electron damping constant are $\gamma \sim 10^{13}$ s^{-1} or larger, so an underdamped electron dynamics would set in only for exceedingly large magnetic fields [16]. A more promising realm for an experimental demonstration of the effect under investigation is a 2D electron gas, where mobility can be quite high, thus corresponding to a small damping constant $\gamma \sim 10^9$ s^{-1}. A relatively low magnetic field (of about 0.1 T) then would easily satisfy the condition $\gamma \ll \omega_c$. However, since the plasma frequency ω_p of an unconstrained 2D electron gas tends to be very low, artificial geometries should be implemented. Helpful in this regard are two sets of recent experiments, which detected, respectively, oscillations in the magnetoresistances of two-dimensional lateral surface superlattices with square patterns [17] and dynamical phase transitions between localized and superdiffusive (or ballistic) regimes for paramagnetic colloidal systems confined to magnetic bubble domains [18]. Both results can be explained, in the semiclassical approximation, as a commensurability effect between the cyclotron radius of the magnetocharges and the spatial periodicity of the substrate, without the need to invoke quantum mechanics.

We finally point out that the diffusion of confined magnetocharged particles is a topic of increasing interest beyond solid state physics. In medical research, for instance, magnetic nanostructures confined to 2D geometries are thought to offer the most exciting avenues to nanobiomagnetic applications, including targeted drug delivery, bioseparation, and cancer therapy, even if their diffusion properties are not yet fully controllable. The possibility of extending our analysis to nanobiomagnetic processes at the cellular level requires advances on at least two issues. The first is diffusion of complex magnetic materials. In biomedical applications, pointlike magnetocharges are often replaced by synthetic magnetic structures such as magnetic microdiscs with a spin-vortex ground state [19]. The second is wall interactions. Contrary to our simple model, the interactions between a magnetocharge and cellular walls are typically inelastic, namely, characterized by finite interaction times, energy transfer, and even structural changes such as the activation on mechanosensitive ion channels. Both issues are the subject of ongoing investigations by research teams worldwide.

ACKNOWLEDGMENTS

F.M. acknowledges partial support from the Seventh Framework Programme under Grant No. 256959, for Project NANOPOWER. S.S. thanks the Alexander von Humboldt Stiftung for a F.W. Bessel research award. P.H. acknowledges financial support from the DFG excellence cluster "Nanosystems Initiative Munich" (NIM).

[1] K. W. Gentle, Rev. Mod. Phys. **67**, 809 (1995).
[2] P. P. Sosenko, Phys. Scr. **50**, 82 (1994).
[3] L. I and J.-M. Liu, Phys. Rev. Lett. **74**, 3161 (1995).
[4] L. Gammaitoni, P. Hänggi, P. Jung, and F. Marchesoni, Rev. Mod. Phys. **70**, 223 (1998).
[5] P. S. Burada, P. Hänggi, F. Marchesoni, G. Schmid, and P. Talkner, ChemPhysChem. **10**, 45 (2009).

[6] P. K. Ghosh, F. Marchesoni, S. E. Savel'ev, and F. Nori, Phys. Rev. Lett. **104**, 020601 (2010).

[7] *Electron Cyclotron Resonance*, edited by F. P. Miller, A. F. Vandome, and J. McBrewster (Alphascript, Mauritius, 2010).

[8] F. F. Chen, *Introduction to Plasma Physics* (Plenum, New York, 1974).

[9] J. B. Taylor, Phys. Rev. Lett. **6**, 262 (1961); B. Kurşunoğlu, Phys. Rev. **132**, 21 (1963).

[10] R. Czopnik and P. Garbaczewski, Phys. Rev. E **63**, 021105 (2001).

[11] J. I. Jiménez-Aquino and M. Romero-Bastida, Phys. Rev. E **74**, 041117 (2006); I. Holod, A. Zagorodny, and J. Weiland, *ibid.* **71**, 046401 (2005); T. P. Simoẽs and R. E. Lagos, Physica A **355**, 274 (2005); L. Ferrari, *ibid.* **163**, 596 (1990).

[12] C. W. Gardiner, *Handbook of Stochastic Methods* (Springer, Berlin, 2004).

[13] P. Hänggi and H. Thomas, Phys. Rep. **88**, 207 (1982).

[14] P. Jung and P. Hänggi, Phys. Rev. A **44**, 8032 (1991).

[15] F. Marchesoni, L. Gammaitoni, and A. R. Bulsara, Phys. Rev. Lett. **76**, 2609 (1996).

[16] A. A. Abrikosov, *Fundamentals of the Theory of Metals* (North-Holland, Amsterdam, 1988).

[17] D. E. Grant, A. R. Long, and J. H. Davies, Phys. Rev. B **61**, 13127 (2000); S. Chowdhury, C. J. Emeleus, B. Milton, E. Skuras, A. R. Long, J. H. Davies, G. Pennelli, and C. R. Stanley, *ibid.* **62**, R4821 (2000).

[18] P. Tierno, T. H. Johansen, and T. M. Fischer, Phys. Rev. Lett. **99**, 038303 (2007); P. Tierno, A. Soba, T. H. Johansen, and F. Saguès, Appl. Phys. Lett. **93**, 214102 (2008).

[19] D. H. Kim, E. A. Rozhkova, I. V. Ulasov, S. D. Bader, T. Rajh, M. S. Lesniak, and V. Novosad, Nature Mater. **9**, 165 (2010).